Shape of a moving fluxon in stacked Josephson junctions

V. M. Krasnov
Department of Microelectronics and Nanoscience, Chalmers University of Technology, S-41296 Göteborg, Sweden and Institute of Solid State Physics, 142432 Chernogolovka, Russia

D. Winkler
Department of Microelectronics and Nanoscience, Chalmers University of Technology, S-41296 Göteborg, Sweden and IMEGO Institute, Aschebergsgatan 46, S41133, Göteborg, Sweden

(Received 22 March 1999; revised manuscript received 2 August 1999)

We study numerically and analytically the shape of a single fluxon moving in double stacked Josephson junctions (SJJ's) for various junction parameters. We show that the fluxon in a double SJJ consists of two components, which are characterized by different Swihart velocities and Josephson penetration depths. The weight coefficients of the two components depend on the parameters of the junctions and the velocity of the fluxon. It is shown that the fluxon in SJJ's may have an unusual shape with an inverted magnetic field in the second junction when the velocity of the fluxon is approaching the lower Swihart velocity. Finally, we study the influence of fluxon shape on flux-flow current-voltage characteristics and analyze the spectrum of Cherenkov radiation for fluxon velocity above the lower Swihart velocity. An analytic expression for the wavelength of Cherenkov radiation is derived. [S0163-1829(99)03642-5]

I. INTRODUCTION

Properties of stacked Josephson junctions (SJJ's) are of considerable interest both for applications in cryoelectronics and for fundamental physics. A particular interest in SJJ's was stimulated by the discovery of high-T_c superconductors (HTSC's). Highly anisotropic HTSC compounds, such as $Bi_2Sr_2CaCu_2O_{8+x}$, may be considered as stacks of atomic scale intrinsic Josephson junctions.[1] The layered structure determines many of the unusual properties of HTSC. The behavior of model low-T_c SJJ's and HTSC's exhibit many similarities.[2] Due to mutual coupling of junctions in the stack, the physical properties of SJJ's can be qualitatively different from those of single Josephson junctions (JJ's). Therefore, a one-to-one comparison between single and stacked Josephson junctions is difficult to do. Hence, the basic properties of SJJ's have to be studied in order to describe correctly the Josephson behavior of layered superconductors.

Perpendicular (c-axis) transport measurements in magnetic field H parallel to layers (ab plane) is an explicit way of studying Josephson phenomena in SJJ's. In this case, magnetic field penetrates the stack in the form of Josephson-type vortices (fluxons), and the c-axis voltage is caused by motion of such fluxons along the layers. The fluxon in SJJ's is different both from Abrikosov vortex in bulk superconductor, since it does not have a normal core, and from Josephson vortex in single JJ, since the circulating currents are not confined within one junction. The behavior of SJJ's becomes particularly complicated when the length of the stack in one direction L is much larger than the Josephson penetration depth λ_J. One of the unusual properties of long SJJ's is the existence of multiple quasiequilibrium fluxon modes,[3] and submodes,[4] which are characterized by different fluxon configurations in the stack. Due to the existence of such modes and submodes, the state of the stack is not well defined by external conditions. Rather it can be described only statistically with a certain probability of being in any of the quasiequilibrium states. Experimental evidences for the existence of such modes were obtained both for HTSC intrinsic SJJ's (Refs. 4–6) and low-T_c multilayers.[7] The existence of fluxon modes and submodes dramatically changes the behavior of long strongly coupled SJJ's with respect to that of single long JJ's. An example of this is the critical current I_c, which becomes multiple valued,[4–6] the fluctuations of I_c become anomalously large,[4,6] and the magnetic field dependence of I_c becomes very complicated without periodicity in H.[4]

For understanding both the static and dynamic properties of SJJ's, the shape of the fluxon in SJJ's is important, and should be determined. In the static case, the shape of the single fluxon was studied for layered superconductors consisting of an infinite number of thin identical[8] or nonidentical[9] layers and for SJJ's.[3,10] In our previous work,[3] we have shown that in double SJJ's, two special single component fluxon solutions exist, which are characterized by different Swihart velocities and Josephson penetration depths. An approximate analytic fluxon solution was suggested as a linear combination of the single component solutions.[3,11] For the static case, the approximate solution was shown to be in a quantitative agreement with numerically obtained solutions. Extending the approximate analytic solution to the dynamic case, it was predicted that drastic changes in the fluxon shape could occur with increasing the fluxon velocity, resulting, e.g., in possible inversion of the sign of the magnetic field in the second junction and appearance of attractive fluxon interaction.[3] On the other hand, the choice between the special single component solutions and the approximate analytic fluxon solution was not addressed and the dependence of the fluxon shape on the junction parameters was not studied. Using the perturbation approach, the second order correction to the approximate analytic solution was derived

and the accuracy of the solution was recently analyzed.[11]

To our knowledge, no comprehensive analysis of the single fluxon shape in SJJ's exists for the dynamic case. The scope of the current paper is to study quantitatively the shape of the moving fluxon in double SJJ's for various junction parameters. Our analysis is based on numerical simulations and analytical treatment of the coupled sine-Gordon equation, which describes physical properties of SJJ's.[10] We show that the single moving fluxon in double SJJ's may be described by both a single component solution and a double component solution, depending on the parameters of the stack and the fluxon velocity. Moreover, the shape of the fluxon may be quite anomalous, with inverted magnetic field in the second junction and with nonmonotonous change of phase.

The paper is organized as follows. In Sec. II, we rewrite the coupled sine-Gordon equation for the case of solitonic fluxon motion and review analytic single fluxon solutions obtained in Refs. 3,11. In Sec. III, we present numerical simulations for frictionless fluxon motion for different parameters of SJJ's and compare those with analytical predictions. We also formulate and verify conditions for observation of different fluxon solutions. In Sec. IV, we discuss implementations of the fluxon shape in experimental situation. In Sec. IV A, we study the influence of a finite damping and simulate current-voltage characteristics. Finally, in Sec. IV B we consider the case of nonsolitonic fluxon motion with the propagation velocity larger than the lower Swihart velocity. We have shown that such fluxon motion is accompanied by plasma wave excitations and derive the expression for the wavelength of such ''Cherenkov'' radiation.

II. GENERAL RELATIONS

We consider a double stack with the overlap geometry, consisting of junctions 1 and 2 with the following parameters: the critical current density J_{ci}, the capacitance C_i, the thickness of the tunnel barrier between the layers t_i, the thickness and London penetration depth of superconducting layers d_i and λ_{Si}, and the length of the stack L. Hereafter, the subscript i on a quantity represents its number. The elements of the stack are numerated from the bottom to the top, so that junction i consists of superconducting layers $i, i+1$, and the tunnel barrier i. The fluxon will be placed in JJ 1, if not stated otherwise.

The physical properties of SJJ's are described by the coupled sine-Gordon equation,[10] which for the double stack with overlap geometry can be written as

$$\begin{vmatrix} \varphi_1'' \\ \varphi_2'' \end{vmatrix} = \begin{vmatrix} 1 & -S_2/\Lambda_1 \\ -S_2/\Lambda_1 & \Lambda_2/\Lambda_1 \end{vmatrix} \times \begin{vmatrix} \sin(\varphi_1) + \ddot{\varphi}_1 + \alpha_1 \dot{\varphi}_1 - \dfrac{J_b}{J_{c1}} \\ \dfrac{J_{c2}}{J_{c1}} \sin(\varphi_2) + \dfrac{C_2}{C_1} \ddot{\varphi}_2 + \alpha_2 \dot{\varphi}_2 - \dfrac{J_b}{J_{c1}} \end{vmatrix}, \quad (1)$$

where $\varphi_{1,2}$ are gauge invariant phase differences in JJ's 1 and 2, the prime and overdots on the quantity represent partial derivatives in space and time, respectively. Space and time are normalized to Josephson penetration depth $\lambda_{J1} = \sqrt{\Phi_0 c/8\pi^2 J_{c1}\Lambda_1}$ and inverted Josephson plasma frequency $\omega_{p1}^{-1} = \sqrt{\Phi_0 C_1/2\pi c J_{c1}}$, respectively, of the single JJ 1. Here Φ_0 is the flux quantum, c is the velocity of light in vacuum and

$$\Lambda_i = t_i + \lambda_{Si} \coth\left(\frac{d_i}{\lambda_{Si}}\right) + \lambda_{Si+1} \coth\left(\frac{d_{i+1}}{\lambda_{Si+1}}\right),$$

$$S_i = \lambda_{Si} \operatorname{cosech}\left(\frac{d_i}{\lambda_{Si}}\right).$$

The last terms in the right hand side of Eq. (1) represent total currents in the JJ's, which consist of superconducting, displacement, and quasiparticle contributions, and J_b represents the bias current density. Viscous damping due to quasiparticle current is characterized by the damping coefficient $\alpha_i = \beta_{ci}^{-1/2}$, where β_{ci} is the McCumber parameter of the single JJ i. The coupling strength in the double SJJ's is described by a coupling parameter $S = S_2/\sqrt{\Lambda_1\Lambda_2}$. The magnetic induction in the stack is equal to[3]

$$B_1 = \frac{H_0}{2(1-S^2)}\left[\varphi_1' + \frac{S_2}{\Lambda_1}\varphi_2'\right],$$

$$B_2 = \frac{H_0}{2(1-S^2)}\left[\frac{S_2}{\Lambda_2}\varphi_1' + \frac{\Lambda_1}{\Lambda_2}\varphi_2'\right], \quad (2)$$

where $H_0 = \Phi_0/\pi\lambda_{J1}\Lambda_1$.

For the solitonlike fluxon motion, the phase differences in the stack remain unchanged in the coordinate frame moving along with the fluxon. Introducing the self-coordinate of the fluxon $\xi = x - ut$, and neglecting damping coefficient, we simplify Eq. (1) and rewrite it as a system of coupled ordinary differential equations (ODE's):

$$\varphi_{1\xi\xi}''\left[\frac{ab-S^2}{1-S^2}\right] = a\sin(\varphi_1) - \frac{J_{c2}S_2}{J_{c1}\Lambda_1}\sin(\varphi_2),$$

$$\varphi_{2\xi\xi}''\left[\frac{ab-S^2}{1-S^2}\right] = b\frac{J_{c2}\Lambda_2}{J_{c1}\Lambda_1}\sin(\varphi_2) - \frac{S_2}{\Lambda_1}\sin(\varphi_1), \quad (3)$$

where

$$a = 1 - \frac{u^2}{c_{01}^2}\frac{C_2\Lambda_2}{C_1\Lambda_1}(1-S^2),$$

$$b = 1 - \frac{u^2}{c_{01}^2}(1-S^2), \quad (4)$$

and $c_{01} = \lambda_{j1}\omega_{p1}$ is the Swihart velocity of the single JJ 1. Comparing Eqs. (1) and (3), it is seen that the task is now reduced to solution of the static problem, but with parameters depending on the fluxon velocity.

Equation (3) has a first integral

$$\frac{1}{1-S^2}\left[b\frac{(\varphi'_{1\xi})^2}{2}+a\frac{\Lambda_1}{\Lambda_2}\frac{(\varphi'_{2\xi})^2}{2}+\frac{S_2}{\Lambda_2}\varphi'_{1\xi}\varphi'_{2\xi}\right]+\cos(\varphi_1)$$

$$+\frac{J_{c2}}{J_{c1}}\cos(\varphi_2)=\mathbf{C}, \tag{5}$$

which reduces to that from Ref. 3 for the static case, $u=0$. Here $\mathbf{C}$ is a constant of the first integral.

A. Special single component solutions

In Ref. 3 it was shown that Eq. (1), linearized with respect to φ_2, allows two special single component solutions of the type

$$\varphi_1(\xi)=F_{1,2}=4\arctan[\exp(\xi/\lambda_{1,2})], \tag{6}$$

$$\sin(\varphi_2)=\kappa_{1,2}^{-1}\sin(\varphi_1),$$

where $\kappa_{1,2}$ are solutions of the quadratic equation.

$$\frac{S_2}{\Lambda_1}\kappa^2+\kappa\left[1-\frac{J_{c2}\Lambda_2}{J_{c1}\Lambda_1}+\frac{u^2}{c_{01}^2}\frac{\Lambda_2}{\Lambda_1}\left(\frac{J_{c2}}{J_{c1}}-\frac{C_2}{C_1}\right)(1-S^2)\right]$$

$$-\frac{J_{c2}S_2}{J_{c1}\Lambda_1}=0. \tag{7}$$

Therefore, for a double SJJ's there exist two characteristic Josephson penetration depths

$$\lambda_{1,2}^2=\frac{\lambda_{j1}^2}{1+\kappa_{2,1}S_2/\Lambda_1}\left(1-\frac{u^2}{c_{1,2}^2}\right) \tag{8}$$

and two characteristic velocities

$$c_{1,2}^2=\frac{c_{01}^2}{1+\kappa_{2,1}(C_2J_{c1}S_2)/(C_1J_{c2}\Lambda_1)}. \tag{9}$$

B. Double component solution

Taking the single component solutions as eigenfunctions of the linearized coupled sine-Gordon equation, an approximate analytic single fluxon solution in JJ 1 was obtained in Ref. 3:

$$\varphi_1=\frac{\kappa_1F_1-\kappa_2F_2}{\kappa_1-\kappa_2},$$

$$\varphi_2=\frac{F_1-F_2}{\kappa_1-\kappa_2}. \tag{10}$$

Here $F_{1,2}$ are the single component solutions, Eq. (6). Recently this solution was rederived more rigorously in Ref. 11. It was shown, that for the static case Eq. (10) gives perfect approximation for φ_1 in the whole space region and for arbitrary parameters of the stack.[11,3] Using the perturbation approach the second order correction to Eq. (10) was obtained in Ref. 11. As it is seen from Eq. (10), the single fluxon in double SJJ's consists of two components. From Eq. (8) it is seen that both components contract with increasing velocity, but the characteristic velocities for the contraction are different for each component and are given by Eq. (9). For identical junctions the contraction of each component is of the Lorentz type; however, the contraction of the fluxon itself is different from Lorentz contraction. This is a consequence of the absence of Lorentz invariance for the coupled sine-Gordon equation. For nonidentical junctions, the parameters $\kappa_{1,2}$, depend on the fluxon velocity and thus contraction of the components is somewhat different from Lorentz contraction. In this case the maximum characteristic velocity should be obtained from the equation $u=c_{1,2}$ and Eqs. (7), (9). By analogy with single JJ's we will refer to the maximum characteristic velocities as Swihart velocities $\tilde{c}_{1,2}$. In the general case, Swihart velocities are equal to[12]

$$\tilde{c}_{1,2}=\frac{\sqrt{2}c_{01}c_{02}}{\sqrt{c_{01}^2+c_{02}^2\pm\sqrt{(c_{01}^2-c_{02}^2)^2+4S^2c_{01}^2c_{02}^2}}}, \tag{11}$$

where $c_{02}=c_{01}\sqrt{C_1\Lambda_1/C_2\Lambda_2}$ is the Swihart velocity of the single JJ 2.

The most crucial changes in the fluxon shape occur as the velocity approaches the lowest Swihart velocity $u\to\tilde{c}_1$. Then the first component is totally squeezed $\lambda_1\to0$ while the contraction of the second component remains marginal; see Eq. (8). In this case the two components become clearly distinguishable: the F_1 component transforms into a steplike function which changes from zero to 2π within the distance λ_1 at the fluxon center, while outside the central region the shape of the fluxon is defined by the F_2 component. From Eq. (10) it follows that

$$\frac{\sin(\varphi_1)}{\sin(\varphi_2)}=\begin{cases}\kappa_2, |x|\gg\lambda_1,\\ -\kappa_1, x\to0\end{cases}\quad(u\to\tilde{c}_1). \tag{12}$$

For $C_2\Lambda_2/C_1\Lambda_1=1$, and $u=\tilde{c}_1$, the parameters $\kappa_{1,2}$ are equal to

$$\kappa_{1,2}=-\sqrt{\frac{\Lambda_1}{\Lambda_2}},\sqrt{\frac{\Lambda_2}{\Lambda_1}\frac{J_{c2}}{J_{c1}}}. \tag{13}$$

The parameters $\kappa_{1,2}$ determine the weight coefficients of the components. From Eqs. (10), (13) it follows that F_1 component dominates for $J_{c2}/J_{c1}\ll1$, and F_2 dominates for $J_{c2}/J_{c1}\gg1$.

From the analysis above, it is seen that the linearized coupled sine-Gordon equation allows both the single component solutions $F_{1,2}$, Eq. (6) and the double component solution, Eq. (10). At this stage it is not clear which of the solutions, Eqs. (6), (10), should be realized in SJJ's, since all three solutions have roughly the same accuracy with respect to Eq. (1). In Refs. 3,11 it was shown that it is the double component solution Eq. (10) which is realized in the static case. However, it was suggested that a single component solution could be achieved at high fluxon velocities. Indeed, as we will show below, in the dynamic case both single and double component solutions can exist and even coexist, depending on parameters of the stack and the fluxon velocity. What is important, however, is that these are always the components $F_{1,2}$ described by Eqs. (6), (7) which constitute the fluxon.

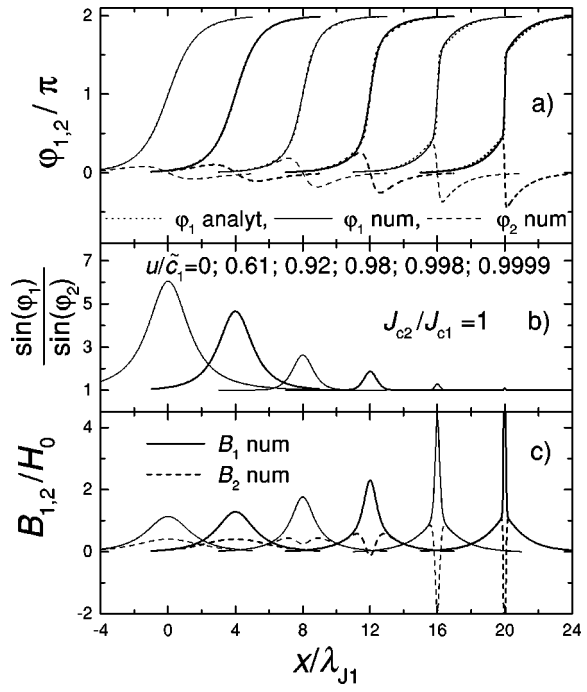

FIG. 1. Profiles of (a) phase differences $\varphi_{1,2}$, (b) the ratio $\sin(\varphi_1)/\sin(\varphi_2)$, and (c) magnetic inductions $B_{1,2}$ of a single fluxon are shown for double SJJ's consisting of identical strongly coupled junctions and for different fluxon velocities $u/\tilde{c}_1 = 0,0.61,0.92,0.98,0.998,0.9999$ (from left to right curve). In (a) dotted lines show profiles obtained from the analytic double component solution Eq. (10). The rest of the curves were obtained numerically. It is seen that the fluxon shape in this case is well described by Eq. (10) and consist of contracted and uncontracted components. The sign inversion of $B_2(0)$ at $u \simeq \tilde{c}_1$ is clearly seen.

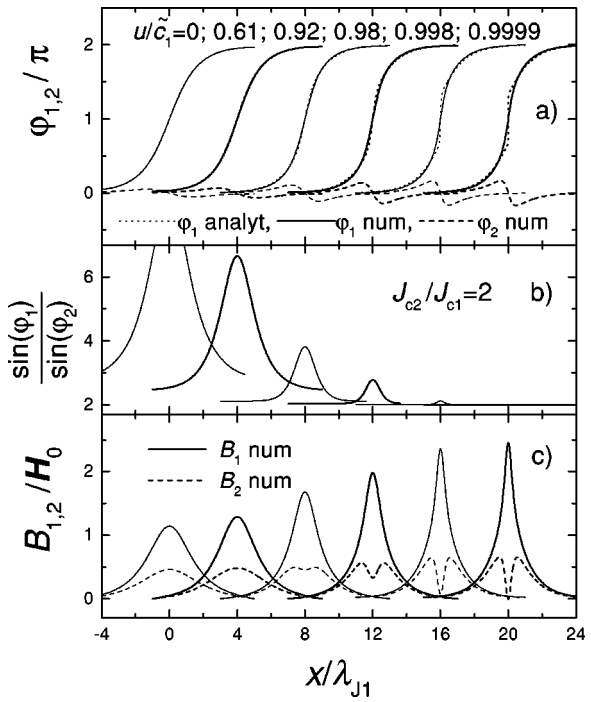

FIG. 2. The same as in Fig. 1 but for $J_{c2}/J_{c1}=2$. The fluxon is placed in the weaker junction. At $u<0.98\tilde{c}_1$, the fluxon is well described by the double component solution, Eq. (10). At higher velocities transformation to the single F_2 component solution, Eq. (6), with $\kappa_2=2$, takes place.

III. FRICTIONLESS CASE

In this section we will consider unperturbed, $\alpha_i=0$, $J_b=0$, frictionless fluxon motion. We analyze the pure solitonic fluxon motion for various junction parameters, make general conclusions about transformation of the fluxon shape in dynamics, and compare it with analytical predictions. We also derive and verify conditions for observation of single and double component fluxon at $u \to \tilde{c}_1$. The effect of finite damping and bias will be considered in Sec. IV. The numerical procedure was based on a finite difference method with successive iterations of ODE, Eq. (3). The boundary conditions were such that the total phase shift is equal to 2π in the junction containing a fluxon and zero in the other one. The fluxon will be placed in JJ 1 if not stated otherwise.

A. Identical junctions: Double component solution

In Fig. 1, profiles of (a) phase differences $\varphi_{1,2}$, (b) the ratio $\sin(\varphi_1)/\sin(\varphi_2)$, and (c) magnetic inductions $B_{1,2}$ of a single fluxon in JJ 1 are shown for a double stack consisting of identical strongly coupled JJ's and for different fluxon velocities $u/\tilde{c}_1=0,0.61,0.92,0.98,0.998,0.9999$ (from left to right curve). The curves were shifted for clarity along the x axis. Parameters of the stack are $d_i=t_i=0.01\lambda_{J1}$, $\lambda_{Si}=0.1\lambda_{J1}$, $S\simeq 0.5$, $C_1=C_2$. In Fig. 1(a) dotted lines show profiles obtained from the analytic double component solution Eq. (10). Solid and dashed lines in Figs. 1(a), 1(c) represent results of numerical simulations for JJ's 1 and 2, respectively. The data in Figs. 1(b), 1(c) are obtained numerically. The magnetic induction is normalized to $H_0=\Phi_0/\pi\lambda_{J1}\Lambda_1$.

As the velocity approaches the lower Swihart velocity $\tilde{c}_1$, the existence of the two fluxon components becomes clearly seen. For identical junctions, as it follows from Eqs. (10), (13), exactly one half of the fluxon belongs to each component. The F_1 contribution transforms to a one-π step. Outside the fluxon center the fluxon is defined entirely by the F_2 component, which is only marginally contracted. Moreover, from Fig. 1(a) it is seen that at $u \sim \tilde{c}_1$ the phase differences in both junctions are equal outside the fluxon center in agreement with analytical prediction, Eq. (12). This is illustrated in Fig. 1(b), from which it is seen that the ratio $\sin(\varphi_1)/\sin(\varphi_2)$ approaches unity as $u \to \tilde{c}_1$. From Fig.1(a) it is seen that the approximate analytic solution is in good agreement with the numerical solutions for all fluxon velocities. Another unusual feature of the moving fluxon in SJJ's is seen from Fig. 1(c). A dip in B_2 is developed with increasing fluxon velocity, leading to inversion of the sign at high velocities.[3] From Eqs. (2), (10) it follows that for identical SJJ's $B_2(0)=-B_1(0)$ at $u=\tilde{c}_1$.

B. Fluxon in a weaker junction: Uncontracted single component solution

Figure 2 shows the case when the fluxon is placed in the weaker junction $J_{c2}/J_{c1}=2$; the rest of the parameters and the way of presentation are the same as in Fig. 1. At veloci-

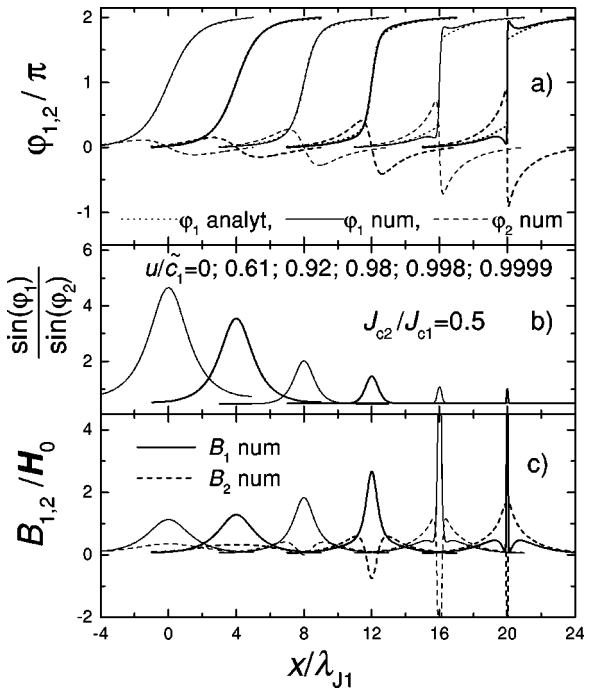

FIG. 3. The same as in Fig. 1 but for $J_{c2}/J_{c1}=0.5$. The fluxon is placed in the stronger junction. At $u<0.98\tilde{c}_1$, the fluxon is well described by the double component solution, Eq. (10). At higher velocities transformation to a more complicated two component solution, Eq. (14), takes place.

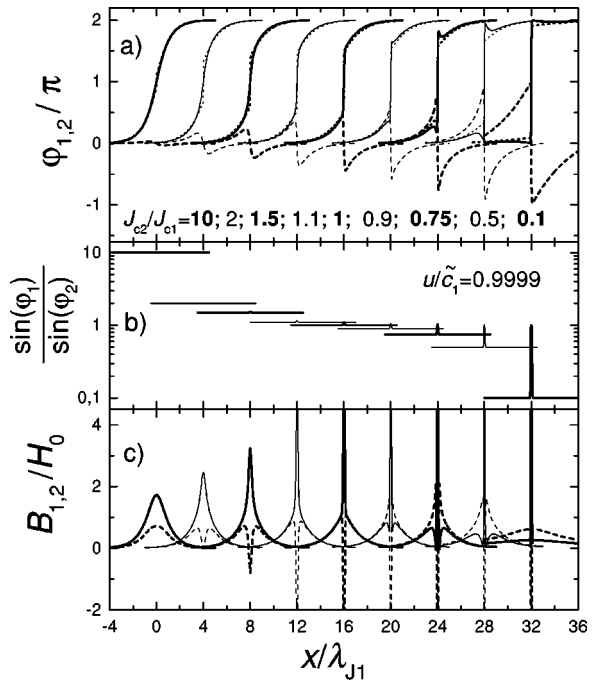

FIG. 4. Profiles of the fluxon moving with $u=0.9999\tilde{c}_1$, for J_{c2}/J_{c1} from 10 to 0.1. From (b) it is seen that single and two component solutions are observed for fluxon in weaker ($J_{c2}/J_{c1}>1$) and stronger ($J_{c2}/J_{c1}<1$) junction, respectively.

ties up to $0.98\tilde{c}_1$ the shape of the fluxon is well described by the double component solution, Eq. (10). At higher velocities, transformation to the single F_2 component solution, Eq. (6), takes place. Indeed, from Fig. 3(b) it is seen that as $u\rightarrow\tilde{c}_1$, $\sin(\varphi_1)/\sin(\varphi_2)\rightarrow\kappa_2=2$ in the whole space region. From Fig. 3(c) it is seen that a dip in B_2 at $u\simeq\tilde{c}_1$ is reduced with respect to that in Fig. 1(c), due to absence of the contracted F_1 component.

C. Fluxon in a stronger junction: Two component solution

Figure 3 shows the case when the fluxon is placed in the stronger junction $J_{c2}/J_{c1}=0.5$; the rest of the parameters and the way of presentation are the same as in Fig. 1. At velocities up to $0.98\tilde{c}_1$, the shape of the fluxon is well described by the double component solution, Eq. (10). At higher velocities the fluxon still has contracted and uncontracted components $F_{1,2}$. The existence of the two fluxon components is clearly seen from Fig. 3(b). As $u\rightarrow\tilde{c}_1$, $\sin(\varphi_1)/\sin(\varphi_2)\rightarrow\kappa_2=0.5$ outside the center of the fluxon and $\sin(\varphi_1)/\sin(\varphi_2)\rightarrow-\kappa_1=1$ in the center, in agreement with Eqs. (12), (13). However, transformation of the fluxon shape with respect to Eq. (10) takes place. From Fig. 3(a) it is seen that in the left half-space the phase shifts in JJ's 1 and 2 approach zero and π, respectively, and belong to the uncontracted F_2 component, as seen from Fig. 3(b). Therefore, there is a single F_2 component fluxon placed in JJ 2 (the weaker junction). The situation in the left half space is then analogous to that in Fig. 2. Indeed, in the left half space $\varphi_{1,2}(x/\lambda_{J2})$ from Fig. 3(a) merge with $\varphi_{2,1}(x/\lambda_{J1})$ from Fig. 2(a). Rescaling of the x axis to λ_{J2} is necessary because the F_2 component is now situated in JJ 2. In the central region, a steplike change of phase shift takes place in both junctions. In JJ 1 the phase jumps on $+2\pi$, which means that there is a single F_1 component fluxon and in JJ 2 the phase drops on -2π, representing the single F_1 component antifluxon. The overall fluxon shape at $u=\tilde{c}_1$ from Fig. 3 can be written as

$$\varphi_1=F_1+\text{image}(\varphi_2),$$
$$\varphi_2=F_2-F_1 \tag{14}$$

so that in JJ 1 there is the contracted single component F_1 fluxon plus an image from JJ 2 in a form of a ripple and in JJ 2 there is uncontracted fluxon F_2 – contracted antifluxon F_1 pair. The total phase shifts in JJ's 1 and 2 are 2π and zero, respectively. However, φ_1 increases nonmonotonously and has two local maxima and minima, see Fig. 3(a). From Fig. 3(c) it is seen that the dip in B_2 in this case is even more pronounced than that for identical SJJ's, Fig. 1(c). This is due to the increase of the weight coefficient of the contracted F_1 component.

Figure 4 shows profiles of the fluxon moving with the velocity very close to the lower Swihart velocity, $u=0.9999\tilde{c}_1$, for different critical current densities J_{c2}/J_{c1} from 10 to 0.1 increasing sequentially from the left to the right curve. The rest of the stack parameters and the way of presentation are the same as in Fig. 1. From Fig. 4 it is seen how the shape of the fluxon is changed with J_{c2}/J_{c1}. When the fluxon is placed in the weaker junction $J_{c2}/J_{c1}>1$, the fluxon shape at $u\simeq\tilde{c}_1$ is described by the single F_2 component. For the case of Figs. 1–4, $C_2/C_1=\Lambda_2/\Lambda_1=1$, so that $\kappa_2=J_{c2}/J_{c1}$. In Fig. 4(b) the dependence $\sin(\varphi_1)/\sin(\varphi_2)=J_{c2}/J_{c1}$ is clearly visible in the whole space region for $J_{c2}/J_{c1}>1$. When the fluxon is placed in the stronger junc-

tion, $J_{c2}/J_{c1}<1$, it has two components, $F_{1,2}$. From Fig. 4(b) it is seen that for the case $J_{c2}/J_{c1}<1$, the fluxon shape in the center is determined by the F_1 component, $\sin(\varphi_1)/\sin(\varphi_2)=-\kappa_1=1$, while outside the center the shape is given by the F_2 component, $\sin(\varphi_1)/\sin(\varphi_2)=\kappa_2=J_{c2}/J_{c1}$, in agreement with Eqs. (12), (13).

From Fig. 4 it is seen that the transition from a double to a single component solution for $J_{c2}/J_{c1}>1$ is gradual. Outside the fluxon center this transition is well described by a gradual increase of the weight coefficient of the F_2 component, Eqs. (10), (13). In the center the exact shape of the fluxon can be obtained from the first integral, Eq. (5). For the case $C_2\Lambda_2/C_1\Lambda_1=1$, at $u=\tilde{c}_1$ the first integral reduces to

$$\frac{S}{1-S^2}\left(1+\frac{J_{c1}\Lambda_1}{J_{c2}\Lambda_2}\frac{\cos(\varphi_1)}{\cos(\varphi_2)}\right)^2\frac{(\varphi'_{1\xi})^2}{2}$$

$$=1-\cos(\varphi_1)+\frac{J_{c2}}{J_{c1}}[1-\cos(\varphi_2)], \qquad (15)$$

for the F_2 single component solution. From Eq. (15) it is seen that at the fluxon center, $x=0$, the effective Josephson penetration depth is equal to

$$\lambda_{\rm eff}(F_2)=\lambda_{J1}\left(1-\frac{J_{c1}\Lambda_1}{J_{c2}\Lambda_2}\right)\sqrt{\frac{S}{1-S^2}}, \qquad (16)$$

so that $\lambda_{\rm eff}$ gradually increases from zero to $\lambda_{J1}\sqrt{S/(1-S)^2}$, as $J_{c2}\Lambda_2/J_{c1}\Lambda_1$ becomes larger than unity. The inequality

$$\frac{J_{c2}\Lambda_2}{J_{c1}\Lambda_1}>1 \qquad (17)$$

is then a necessary (but as we will show below not sufficient) condition for the existence of the single component F_2 solution at $u=\tilde{c}_1$, for $C_2\Lambda_2/C_1\Lambda_1=1$, since then $\lambda_{\rm eff}$ remains finite at $u=\tilde{c}_1$.

On the other hand, the transition from the double component solution, Eq. (10), to the solution, Eq. (14), for $J_{c2}/J_{c1}<1$ is sharp. However, the closer J_{c2}/J_{c1} is to unity, the closer the fluxon velocity to $\tilde{c}_1$ must be in order to observe this transformation, as it can be seen from Figs. 3, 4.

D. Nonidentical electrodes: Bifurcations and more complicated two component solutions

So far we have considered the case when only critical current densities of SJJ's were different. Another common type of nonuniformity in SJJ's is the difference in electrodes. Figure 5 shows fluxon shape for the case, $\Lambda_2\simeq 2.5\Lambda_1$. Physically this means that the third electrode has either larger London penetration depth, $\lambda_{S3}=2\lambda_{J1,2}$, or it is thinner than the rest of the electrodes, $d_{1,2}=4d_3$, see definitions in Sec. II. The rest of the parameters are $J_{c2}/J_{c1}=0.5$, $d_{1,2}=t_i=0.01\lambda_{J1}$, $\lambda_{S1,2}=0.1\lambda_{J1}$, $S\simeq 0.31$, $C_2\Lambda_2/C_1\Lambda_1=1$. The way of presentation is the same as in Fig. 1. At velocities up to $0.98\tilde{c}_1$, the fluxon is well described by the analytic double component solution, Eq. (10). From Fig. 5(b) it is seen that outside the fluxon center the phase distribution is determined by the F_2 component with $\kappa_2\simeq 0.79$, given by Eq. (13).

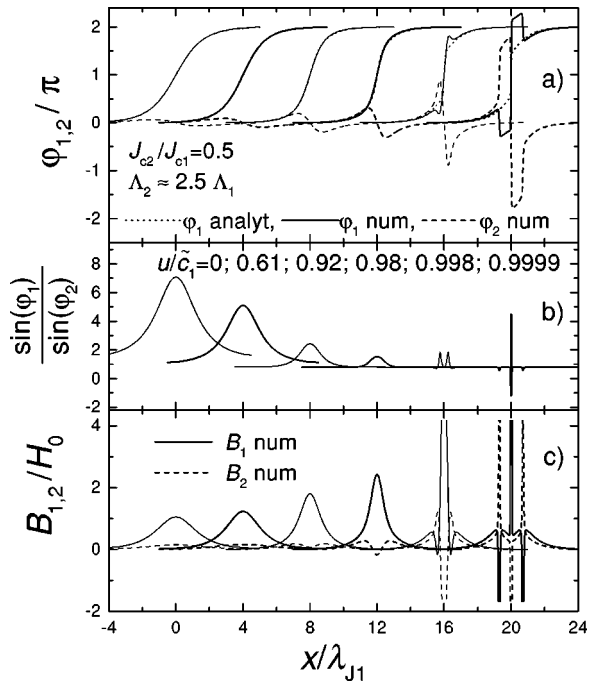

FIG. 5. Fluxon shape for the case of nonidentical electrodes $\Lambda_2\simeq 2.5\Lambda_1$ and $J_{c2}/J_{c1}=0.5$. The rest of the parameters and the way of presentation is the same as in Fig. 1. At u up to $0.98\tilde{c}_1$, the fluxon is well described by the double component solution, Eq. (10). However, at $u>0.998\tilde{c}_1$ switching to two different types of solutions, Eqs. (14), (18), occur.

However, at $u\sim 0.998\tilde{c}_1$ the system exhibits bifurcations and a sudden switching to the solution given by Eq. (14) occurs. At slightly larger velocity another bifurcation takes place resulting in switching to yet another solution. The switching between the solutions is hysteretic. If we start reducing the fluxon velocity, the switching back takes place at somewhat lower velocity. Therefore, there is a certain region of fluxon velocities for which those solutions coexist.

Looking at the fluxon shape at $u=0.9999\tilde{c}_1$ from Fig. 5 we see that it consists of three parts: (i) at the fluxon center, $x=0$, in JJ 1 there is a 2π step, which as we will show in a moment, belongs to the pure F_1 component and in JJ 2 there is a 4π drop belonging to two flux quantum $-2F_1$ antifluxon. (ii) At $x=x_0\simeq 0.7\lambda_{J1}$ and (iii) $x=-x_0$, in JJ 2 there is a 2π increase and in JJ 1 there is a ripplelike phase shift. As it can be seen from Figs. 5(a), 5(c), the features at $x=\pm x_0$ contain both contracted and uncontracted parts and are in fact given by the double component solutions, Eq. (10). This is illustrated in Fig. 6(a) in which solid and dashed lines show phase distributions φ_1 and φ_2, respectively, from Fig. 5(a) for $u=0.9999\tilde{c}_1$ and dashed-dotted and dotted curves represent φ_1 and φ_2, respectively, given by the analytic double component solution, Eq. (10), shifted by $-x_0$ along the x axis. Obviously, the features at $x=\pm x_0$ correspond to the double component soliton placed in JJ 2. Due to spatial separation between the contracted centrum of the fluxon and the double component features at $x=\pm x_0$, we can analyze the shape of the central contracted part. From Fig. 5(c) it is seen that $B_1(0)$ increases sharply as the velocity approaches $\tilde{c}_1$. If the phase distribution in the central region is given by

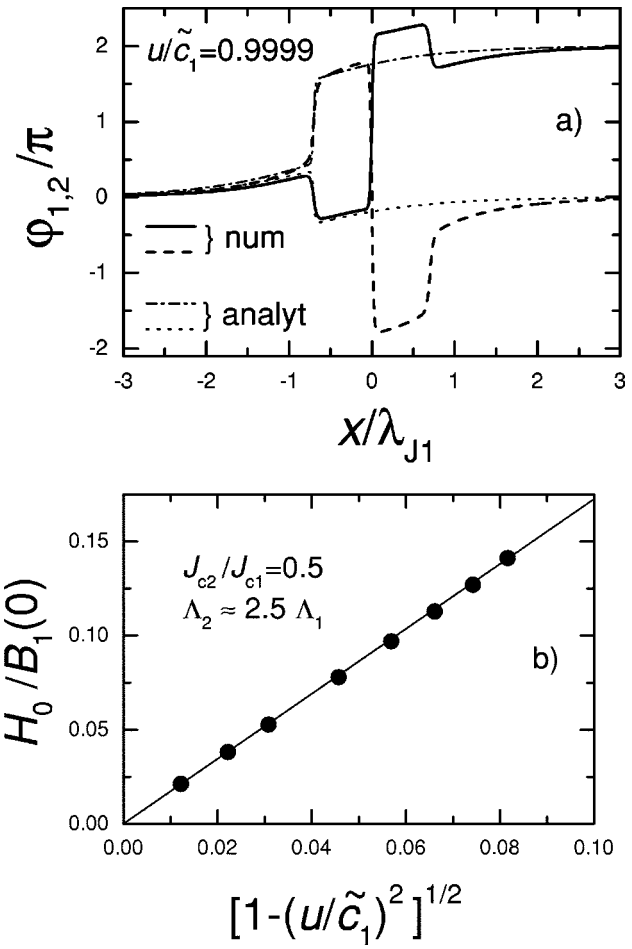

FIG. 6. (a) Soliton shape at $u=0.9999\tilde{c}_1$ from Fig. 5. Solid and dashed lines represent $\varphi_{1,2}$ obtained from numerical simulation, while dashed-dotted and dotted lines represent the analytic double component solution in JJ 2, shifted by $x=-x_0$. (b) Inverted values of magnetic induction in the center of JJ 1 versus the Lorentz factor. Symbols represent numerical simulations and solid line is an apparent linear fit. Clear Lorentz contraction of the central region at $u=\tilde{c}_1$ is seen.

the F_1 component, then according to Eq. (2), $B_1(0)\sim\lambda_1^{-1}\sim(1-u^2/\tilde{c}_1^2)^{-1/2}$. Figure 6(b) shows the inverse value of $B_1(0)$ versus the Lorentz factor $(1-u^2/\tilde{c}_1^2)^{1/2}$, for the high velocity solution from Fig. 5. Dots represent the numerically obtained values, solid line is the apparent linear fit. The Lorentz contraction of the central region at the lowest Swihart velocity, $\tilde{c}_1$, is clearly seen, therefore confirming that the central region is given by the pure F_1 component. The soliton in this case can be described as

$$\varphi_1=F_1+\text{image}(\varphi_2),$$
$$\varphi_2=\varphi_{dcs}(x-x_0)-2F_1+\varphi_{dcs}(x+x_0), \qquad (18)$$

where φ_{dcs} is the double component solution, Eq. (10). The overall phase shift is 2π in JJ 1 and zero in JJ 2; however, the phase growth is nonmonotonous in JJ 1.

E. Conditions for the existence of single and two component solutions

For practical applications of SJJ's in flux-flow oscillators, the shape of the fluxon at the highest propagation velocity is

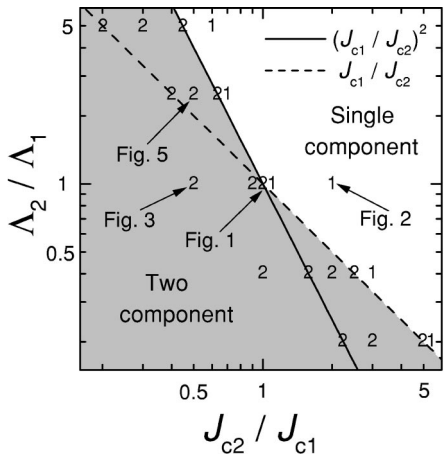

FIG. 7. Regions of existence of the two component (shaded area) and the single component solutions at $u=\tilde{c}_1$ for $C_2\Lambda_2/C_1\Lambda_1=1$. Numbers indicate the number of components, obtained numerically. Solid and dashed lines represent the conditions Eq. (19) and Eq. (17), respectively. It is seen that the single component solution exists when both conditions are satisfied.

crucial. It is then important to know how the shape of the fluxon at $u=\tilde{c}_1$ depends on the parameters of the stack. Equation (17) formulates the necessary condition for the existence of uncontracted single component F_2 solution at $u=\tilde{c}_1$, for $C_2\Lambda_2/C_1\Lambda_1=1$, since then λ_{eff} remains finite at $u=\tilde{c}_1$. However this condition is not sufficient. Indeed, for the case of Fig. 5, $J_{c2}\Lambda_2/J_{c1}\Lambda_1\simeq 1.25$, i.e., Eq. (17) is satisfied. However, we obviously do not observe the single component F_2 solution at $u=\tilde{c}_1$, but rather a switching to more complicated two component solutions, Eqs. (14), (18), takes place. This happens when the maximum of φ_2 approaches $\pi/2$. If the solution was to stay at the special single component F_2 solution, then according to Eq. (6), the maximum value of $\sin(\varphi_2)$ would be equal to $1/\kappa_2$. This gives us an additional condition for the observation of the single component F_2 solution:

$$\kappa_2>1. \qquad (19)$$

In Fig. 7, regions of the existence of the two component (shaded area) and the single component F_2 solutions at $u=\tilde{c}_1$ are shown for $C_2\Lambda_2/C_1\Lambda_1=1$. The numbers in Fig. 7 show the number of components obtained numerically. Solid and dashed lines represent the conditions Eq. (19) and Eq. (17), respectively. Arrows indicate the cases considered in Figs. 1,2,3,5. It is seen that the single component solution exists when both conditions, Eqs. (17), (19), are satisfied.

IV. IMPLEMENTATION FOR EXPERIMENTAL SITUATION

In the previous section we have studied the unperturbed fluxon motion, $\alpha_i=0, J_b=0$. This is an idealized case. In real experimental situation $\alpha_i\neq 0$ and $J_b\neq 0$. To quantitatively study the influence of damping and bias on the fluxon shape and current-voltage characteristics (IVC's), we performed numerical simulation of the coupled sine-Gordon equation, Eq. (1), with the dissipation and bias terms. Here we used

two approaches: (i) Considering solitonic-type fluxon motion, $\varphi_i=\varphi_i(\xi)$, we derived the ODE system, similar to Eq. (3), but with dissipation and bias terms and used the same numerical procedure to solve it. (ii) Alternatively, we directly integrated the system of partial differential equations (PDE), Eq. (1) using explicit finite difference method. Both approaches have certain advantages and disadvantages. Using ODE, it is possible to calculate fluxon shape for arbitrary small damping, while PDE require relatively large damping coefficient. In addition, ODE in comparison to PDE, does not require a long relaxation and averaging times and does not have problem with accumulation of the error. For solitonic fluxon motion, both approaches give identical results. On the other hand, ODE are restricted to the study of the solitonic motion, while PDE allow more complicated solutions. For simulation of PDE, periodic boundary conditions were used, which correspond to fluxon motion in annular SJJ's with $L=10-100\lambda_{J1}$.

A. Effect of damping and current-voltage characteristics

First of all, fluxon shape will affect the shape of IVC's caused by fluxon motion in the stack.[14] The IVC is determined by a balance between the input power to the system from the current bias source and the power dissipated due to a finite damping, see, e.g., Ref. 15. In single JJ's, Lorentz contraction takes place as the fluxon velocity approaches the Swihart velocity and the fluxon energy increases sharply. The fluxon velocity asymptotically approaches the Swihart velocity with increasing current. In the IVC this result in appearance of an almost vertical step at the velocity matching condition.[15] Since the existence of this step is closely related to the Lorentz contraction of the fluxon, we expect that the step at the velocity matching condition $u=\tilde{c}_1$ should also exist in SJJ's, whenever the fluxon contains the Lorentz contracted part F_1. On the other hand, when a pure F_2 component solution takes place, the fluxon will reach $u=\tilde{c}_1$ at a finite current and flux-flow IVC should have a finite slope at $u=\tilde{c}_1$. For the case when the transformation of the fluxon shape given by Eqs. (14), (18) takes place, this would result in a premature switching from the flux-flow branch and, possibly, in the existence of an extra metastable flux-flow branch in the IVC with the same limiting velocity, $u=\tilde{c}_1$, but with larger dissipation.

The average DC voltage in JJ 1 is $V_1/V_{01}=u/c_{01}$, where $V_{01}=\hbar\pi c_{01}/2eL$, and in JJ 2 is zero. Therefore, we now plot current-velocity characteristics to represent IVC's.

In Fig. 8, the single fluxon IVC's are shown for double SJJ's with equal damping coefficients $\alpha_{1,2}=0.05$, and for $J_{c2}/J_{c1}=1$ (solid diamonds), $J_{c2}/J_{c1}=0.5$ (open circles), $J_{c2}/J_{c1}=2$ (open squares). The rest of parameters are the same as in Fig. 1. Symbols represent solutions obtained from ODE and subsequent solid lines show solutions of PDE, dashed gray line shows the IVC of an uncoupled single JJ 1 and dotted line indicates the position of the lower Swihart velocity, $\tilde{c}_1\simeq 0.817c_{01}$. The insets in Fig. 8 show spatial distribution of $\sin(\varphi_1)$ (solid lines) and $\sin(\varphi_2)$ (dashed lines), for maximum propagation velocities, for which ODE based numerical procedure converged $u_{\max}(J_{c2}/J_{c1}=1)\simeq 0.999\tilde{c}_1$, $u_{\max}(J_{c2}/J_{c1}=0.5)\simeq 0.97\tilde{c}_1$, $u_{\max}(J_{c2}/J_{c1}=2)\simeq 0.99\tilde{c}_1$. The

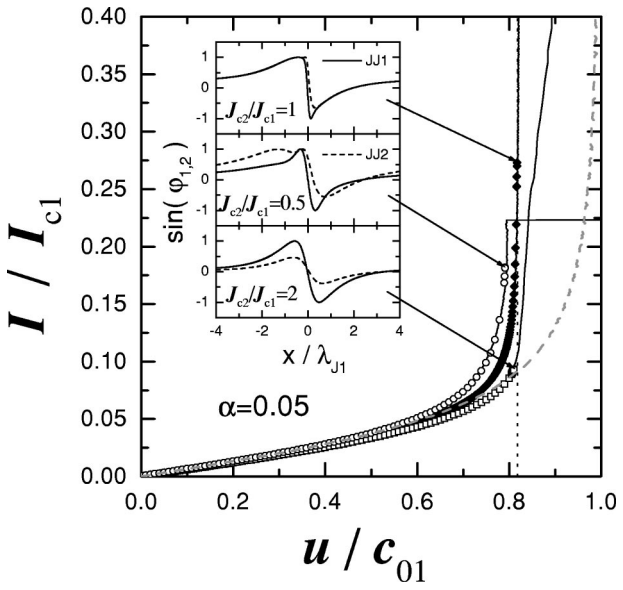

FIG. 8. Single fluxon IVC's are shown for double stack with equal damping, $\alpha_{1,2}=0.05$, and for $J_{c2}/J_{c1}=0.5$, 1, and 2. The rest of parameters are the same as in Fig. 1. Symbols and solid lines represent solutions of ODE and PDE, respectively. Dashed gray line shows the IVC of a single JJ 1 and dotted line indicates $\tilde{c}_1$. Insets show spatial distribution of $\sin(\varphi 1,2)$, for maximum propagation velocities.

solid lines in Fig. 8 show that PDE allow solutions propagating with even larger velocities; however, those solutions are not of solitonic type, and will be discussed in the next section. From Fig. 8 it is seen that the IVC's for $J_{c2}/J_{c1}=1$ and 0.5, exhibit velocity matching behavior at $u\to\tilde{c}_1$. On the other hand, for $J_{c2}/J_{c1}=2$, no velocity matching behavior is observed, and the velocity reaches $\tilde{c}_1$ at a finite current. Such behavior is in agreement with the absence of contracted F_1 component, as discussed above. From the insets in Fig. 8 it is seen, that the fluxon shape for the case of small damping does not differ much from the frictionless case, considered in the previous section. On the other hand, damping reduces the stability of the fluxon state at high propagation velocities, so that the maximum fluxon velocity for pure solitonic motion becomes less than $\tilde{c}_1$. This is due to the finite bias current in the stack, which results in an asymmetry of phase distribution in the stack. Such asymmetry is clearly seen from the inset in Fig. 8 for $J_{c2}/J_{c1}=0.5$. The reduction of stability in the flux-flow state depends on parameters of the stack. For example, for the case of double stack with nonidentical junctions, flux-flow state is more stable for fluxon in the weaker junction $J_{c2}/J_{c1}=2$ than for fluxon in the stronger junction, $J_{c2}/J_{c1}=0.5$. For the case $J_{c2}/J_{c1}=0.5$, switching of the second junction to the quasiparticle branch occurs first at $I/I_{c1}\simeq 0.22$.

In real life, junctions in the stack are not prenumerated and if they are not identical, the stable state will correspond to a fluxon placed in the weaker JJ. Therefore, whenever properties of JJ's in the stack are considerably different, the stable dynamic state at $u=\tilde{c}_1$ would correspond to the existence of uncontracted F_2 component soliton in the weaker JJ. Experimentally, steps at the velocity matching condition were observed for low-T_c SJJ's;[17,18] on the other hand, for

high-T_c intrinsic SJJ's the flux-flow IVC's have a finite slope.[19] We note that for stacks with large number of JJ's with thin electrodes $d \ll \lambda_s$, it is not necessary to have a variation in J_{ci} to make the JJ's different. In this case the middle JJ's have a lower critical field H_{c1}, approximately half of that compared to the outmost JJ's due to the fact that fluxon in the outmost junctions carries only half a flux quantum. In a double stack, considered here, a corresponding thing happens when the JJ's have different electrode thicknesses. The junction with thicker electrodes may have lower H_{c1} even if J_c is larger.[3] In a sense, the criterion for transition from ''weak'' to ''strong'' junction is given by Eqs. (17), (19).

Although the stable state corresponds to the case when fluxon is placed in the weaker JJ, the situation when the fluxon is placed in the stronger JJ can also be achieved in experiment.[18] Obviously such state can be achieved in annular SJJ's. In this case the fluxon can eventually be introduced in the stronger junction and if so it will stay there and can be accelerated by the bias current.

B. Velocity above $\tilde{c}_1$: ''Cherenkov'' radiation

So far we have considered the case $u \leqslant \tilde{c}_1$. For $u > \tilde{c}_1$, coefficients before the second derivative of phase in Eq. (3) become negative. The equation can still be written in a sine-Gordon type form if we substitute $\varphi(\xi) = \pi + \phi(\xi)$. Indeed, a 2π solitonlike solution for $\phi(\xi)$, moving with $u > \tilde{c}_1$, does exist. However the energy of this state is decreasing with increasing velocity and therefore such state would correspond to unstable IVC branch with negative resistance.

In Ref. 3 it was suggested that for $u > \tilde{c}_1$ the fluxon is a combination of a soliton with Josephson plasma waves. From Eq. (8) it is seen that λ_1 becomes imaginary for $u > \tilde{c}_1$ and the F_1 component transforms into a traveling Josephson plasma wave. The fluxon solution is then given by the F_2 component soliton accompanied by Josephson plasma waves from the degenerate F_1 component. Recently, the existence of such type of solution was shown by numerical simulation in Ref. 20 and was interpreted as Cherenkov radiation in SJJ's, when fluxon velocity exceeds the phase velocity of electromagnetic waves. This solution is not of soliton type and cannot be obtained from ODE. Therefore solution of full PDE, Eq. (1), is required. From Fig. 8 it is seen that for the case $J_{c2}/J_{c1} = 2$, PDE allow solutions propagating with $u > \tilde{c}_1$.

In Fig. 9, results of numerical simulations of PDE are shown for $J_{c2}/J_{c1} = 2$, and $u > \tilde{c}_1$. The parameters of SJJ's are the same as in Fig. 8. The insets show spatial distributions of $\sin(\varphi_1)$ (solid lines) and $\sin(\varphi_2)$ (dashed lines) for (a) $u/\tilde{c}_1 \simeq 1.015$, $I/I_{c1} = 0.15$ and (b) $u/\tilde{c}_1 \simeq 1.155$, $I/I_{c1} = 0.5$. Simulations were done for annular SJJ's with $L = 100\lambda_{J1}$. From our simulations we observe that fluxon shape changes gradually as u exceeds $\tilde{c}_1$. Therefore, there are no peculiarities at $u = \tilde{c}_1$ in the IVC, see solid line in Fig. 8 for $J_{c2}/J_{c1} = 2$. Indeed, from inset (a) in Fig. 9 it is seen that for u slightly above $\tilde{c}_1$, fluxon shape in the left halfspace is similar to that at $u < \tilde{c}_1$, see the bottom inset in Fig. 8. However, small oscillations appear behind the fluxon (fluxon is propagating from right to left). As the velocity increases, both amplitude and wavelength of the oscillations increase, as illustrated in inset (b) in Fig. 9. To clarify the physical origin of the oscillations, in Fig. 9 we have plotted the average wavelength of oscillations (circles) as a function of the absolute value of the Lorentz factor, $\sqrt{(u/\tilde{c}_1)^2 - 1}$. The solid line in Fig. 9 shows the absolute value, $2\pi|\lambda_1|$, given by Eq. (8), describing small amplitude plasma waves from the degenerate F_1 component (the factor 2π is due to different definition of the wavelength and the penetration depth). Excellent agreement between the wavelength of oscillations and Josephson plasma wavelength from the degenerate F_1 component is observed without any fitting, thus confirming the idea of Ref. 3 that ''Cherenkov'' radiation is due to plasma wave generation from the degenerate F_1 component. We would like to note that $|\lambda_1|$ is not linear as a function of the Lorentz factor, although deviations from the linear dependence are small. For high propagation velocities, an uncertainty appears in determination of λ. This is caused by the increase of the amplitude of oscillations; see inset (b) in Fig. 9. Here oscillations are not exactly monochromatic but the wavelength slightly increases with the amplitude. The uncertainty in determination of λ at high velocities is shown by error bars in Fig. 9.

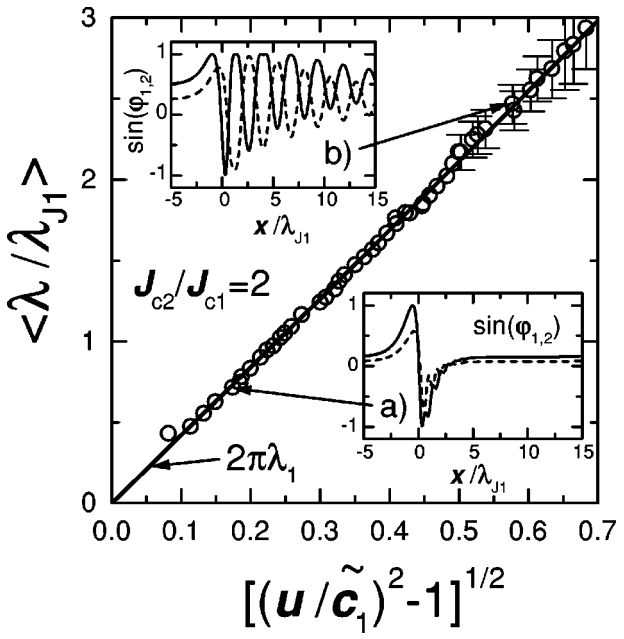

FIG. 9. The wavelength of Cherenkov oscillations (circles) is shown as a function of the absolute value of the Lorentz factor. The solid line represents wavelength $2\pi|\lambda_1|$, for plasma waves from the degenerate F_1 component, given by Eq. (8). Insets show spatial distributions of $\sin(\varphi_1)$ (solid lines) and $\sin(\varphi_2)$ (dashed lines) for (a) $u/\tilde{c}_1 \simeq 1.015$, $I/I_{c1} = 0.15$ and (b) $u/\tilde{c}_1 \simeq 1.155$, $I/I_{c1} = 0.5$, respectively.

V. CONCLUSIONS

In conclusion, we have shown that the shape of a single fluxon in double stacked Josephson junctions can be described by the existence of two components given by Eqs. (6), (7) and with characteristic lengths and velocities given

by Eqs. (8), (9). At velocities up to $u \sim 0.98\tilde{c}_1$, the fluxon is well described by the approximate double component solution, Eq. (10), for all studied junction parameters. In the very vicinity of the lower Swihart velocity, the fluxon shape may undergo radical transformations. The final shape of the fluxon at $u=\tilde{c}_1$ strongly depends on parameters of the stack. From our numerical simulations we have found that the fluxon may remain double component, as shown in Fig. 1, transform to a pure F_2 component solution (see Fig. 2) or be a more complicated combination of F_1 and F_2 components; see Eqs. (14), (18) and Figs. 3,5. Those more complicated solutions do not, strictly speaking, represent the single fluxon state, but are combinations with fluxon-antifluxon pairs. However, even in this case these are always the components $F_{1,2}$ described by Eqs. (6), (7) that constitute the solution. This implies that the components $F_{1,2}$ are real and may live their own life and appear in different combinations. Conditions for observing the single and the two-component solutions at $u=\tilde{c}_1$ were formulated and verified. We have shown that as the velocity approaches $\tilde{c}_1$, the phase shift may become nonmonotonous.

A prominent feature of a soliton moving at the velocity close to $\tilde{c}_1$ in SJJ's is the possible inversion of magnetic field $B_2(0)$. Such a behavior was predicted analytically in Ref. 3. Here we confirmed the existence of this phenomenon by numerical simulation. The inversion of magnetic field in JJ 2 may lead to attractive fluxon interaction for fluxons in different junctions. Then the so-called ''in-phase'' or ''bunched'' state[10] with fluxons one on the top of the other in adjacent junctions may become favorable at high enough fluxon velocity. In experiment, this would result in appearance of an extra flux-flow branch in the current-voltage characteristics with higher voltage, as shown by numerical simulations[16] and observed in experiment on low-T_c SJJ's.[17] In Ref. 13 it was shown that the bunched state can be stable at $u>\tilde{c}_1$; however, no mechanism for overcoming the mutual fluxon repulsion and transformation into the bunched state was suggested. The existence of the field inversion might be a criterion for the appearance of the bunched state in SJJ's. As we have shown, the sign inversion and a dip in $B_2(0)$ disappears when JJ 2 becomes considerably stronger than JJ 1 and transformation of the fluxon shape to a single F_2 component solution takes place; see Fig. 2(c).

The shape of the flux-flow IVC's was analyzed for various parameters of SJJ's and it was shown that velocity matching behavior at $u=\tilde{c}_1$ is observed when fluxon contains the contracted F_1 component. Finally, oscillations at $u>\tilde{c}_1$ were shown to be due to generation of plasma waves from the degenerate F_1 component in agreement with the prediction of Ref. 3. An analytic expression for the wavelength of such ''Cherenkov'' radiation is derived.

ACKNOWLEDGMENTS

The work was supported by Swedish Superconductivity Consortium and in part by the Russian Foundation for Basic Research under Grant No. 96-02-19319.

[1] R. Kleiner *et al.*, Phys. Rev. Lett. **68**, 2394 (1992); Phys. Rev. B **49**, 1327 (1994).
[2] R. Kleiner, P. Müller, H. Kohlstedt, N.F. Pedersen, and S. Sakai, Phys. Rev. B **50**, 3942 (1994).
[3] V.M. Krasnov and D. Winkler, Phys. Rev. B **56**, 9106 (1997).
[4] V.M. Krasnov, N. Mros, A. Yurgens, and D. Winkler, Physica C **304**, 172 (1998).
[5] V.M. Krasnov, N. Mros, A. Yurgens, D. Winkler, and T. Claeson, Appl. Supercond. **6**, 777 (1999).
[6] N. Mros, V.M. Krasnov, A. Yurgens, D. Winkler, and T. Claeson, Phys. Rev. B **57**, R8135 (1998); N. Mros *et al.*, Czech. J. Phys. **46**, 1273 (1996).
[7] V.M. Krasnov, A.E. Kovalev, V.A. Oboznov and N.F. Pedersen, Phys. Rev. B **54**, 15 448 (1996).
[8] J. Clem and M. Coffey, Phys. Rev. B **42**, 6209 (1990).
[9] V.M. Krasnov, N.F. Pedersen, and A.A. Golubov, Physica C **209**, 579 (1993).
[10] S. Sakai, P. Bodin, and N.F. Pedersen, J. Appl. Phys. **73**, 2411 (1993).
[11] V.M. Krasnov, Phys. Rev. B **60**, 9313 (1999).
[12] E. Goldobin, A. Golubov, and A.V. Ustinov, Czech. J. Phys. **46**, 663 (1996).
[13] N. Grønbech-Jensen, D. Cai, and M.R. Samuelsen, Phys. Rev. B **48**, 16 160 (1993).
[14] Strictly speaking, we are talking about fluxon steps in annular SJJ's and zero-field steps.
[15] D.W. McLaughlin and A.C. Scott, Phys. Rev. A **18**, 1652 (1978).
[16] A. Petraglia, A.V. Ustinov, N.F. Pedersen, and S. Sakai, J. Appl. Phys. **77**, 1171 (1994).
[17] S. Sakai, A.V. Ustinov, H. Kohlstedt, A. Petraglia, and N.F. Pedersen, Phys. Rev. B **50**, 12 905 (1994).
[18] R. Monaco, A. Polcari, and L. Capogna, J. Appl. Phys. **78**, 3278 (1995).
[19] J. Ung Lee *et al.*, Appl. Phys. Lett. **67**, 1471 (1995); Physica C **277**, 7 (1997).
[20] E. Goldobin, A. Wallraff, N. Thyssen, and A.V. Ustinov, Phys. Rev. B **57**, 130 (1998).